IEEE Access
Multidisciplinary | Rapid Review | Open Access Journal

Received 1 December 2022, accepted 15 December 2022, date of publication 27 December 2022,
date of current version 20 January 2023.

Digital Object Identifier 10.1109/ACCESS.2022.3232666

RESEARCH ARTICLE

Waveguide Analysis of Radiofrequency Transmission in Well Tubulars for Electromagnetic Heating of Heavy Oil

ADAMU A. ADAMU, (Student Member, IEEE), PRASHANT S. JADHAWAR, AND SUMEET S. APHALE, (Senior Member, IEEE)
School of Engineering, Fraser Noble Building, King's College, Old Aberdeen, AB24 3UE Aberdeen, U.K.

Corresponding author: Sumeet S. Aphale (s.aphale@abdn.ac.uk)

This work was supported by the Nigerian Petroleum Technology Development Fund (PTDF).

ABSTRACT This paper presents the numerical modelling and simulation of a 2D vertical well tubular model excited by a coaxial radiofrequency transmission line placed in its annular space for the purpose of downhole RF energy transmission. The study identifies the mechanism of energy losses due to coupling between the transmission line and steel tubing and casing using resonance mode analysis. The design of a left-handed artificial power line is proposed to minimize the losses due to the right-handed properties of the coaxial transmission line. The design utilizes ideal lumped element method to determine the left-handedness of the right-handed coaxial transmission line over the industrial heating radio-frequency band. The model is developed and simulated using COMSOL multi-physics commercial simulation software. The effect of transmission line position within the annular space on the tangential magnetic field and resulting power losses along the tubing is discussed. It is observed that the resulting artificial power line improves RF power transmission over 60 m depths of the vertical oil well within the industrial heating radiofrequency band.

INDEX TERMS Electromagnetic heating, EM waves, enhanced oil recovery, heavy oil, metamaterials, open-hole completion, radiofrequency, resonance, well tubulars.

I. INTRODUCTION

The depletion of conventional oil reserves has led to the exploration of alternatives such as heavy oil reserves. Most heavy oil and natural bitumen are alteration products of conventional oil. The total resources of heavy oil in known accumulations are 3,396 billion barrels of original oil in place (OOIP), of which 30 billion barrels are included as prospective additional oil. The resource is distributed in 192 basins containing heavy oil [1]. Radiofrequency electromagnetic heating (RF-EMH) has been proposed as an electrothermal enhanced oil recovery (EEOR) method to lower the viscosity of heavy oil [2], [3], [4], [5], [6]. The concept is based on an earlier patent [7], which proposed the propagation of electromagnetic waves to achieve heating by dielectric polarization of polar molecules [8]. Since then, RF-EMH systems have been applied in nuclear fusion [9], [10], [11], food processing [12], [13], [14], and at higher frequencies for medical treatment of cancer [15], [16], [17]. The potential for RF-EMH in EEOR has been established in simulation studies [8], [18], [19], [20], [21], experiments [22], [23], [24] and field tests [25], [26]. These studies have identified the dependency of the method on optimization of input power and operational frequency to achieve high penetration depths for volumetric heating [27], [28]. Furthermore, antenna arrays have been proposed for directional heating based on dipole antennas [29], [30]. Although the field tests mainly utilized frequencies of (1−13.56) MHz and a power range of (5−330) kW, simulation studies have focused on microwave frequencies (> 300) MHz [8]. Electrical energy required for thermal stimulation of heavy oil reservoir formations can be generated from renewable energy sources (RES). Solar, wind and geothermal RES have been investigated for power generation in oil exploration and production [31], [32]. Despite this

The associate editor coordinating the review of this manuscript and approving it for publication was Renato Ferrero.

advantage and previous efforts, the adoption of RF-EMH is still far. To achieve effective performance of the RF-EMH in EEOR, certain conditions serve as guidelines for the design of a feasible regime. Due to the prevalence of vertical oil wells in the industry, their consideration in the design of RF-EMH is paramount. In a single vertical well, the receiving medium (reservoir formation) of cross-sectional diameter d ($50 \leq d \leq 100$) m of the producing well must be heated with a power density of $(1-10)$ kW/m. Depending on the reservoir composition, a power delivery sequence must be established continuously over a significant period of $(2-3)$ years. The means for delivering the power must minimize energy losses in the well structure and unproductive layers of the formation. Additionally, RF antennas should target reservoir pay-zone layer for optimal energy utilization. A balance of desired temperature and penetration should be maintained since temperature change of $(50-100)$ K is sufficient to lower viscosity and stimulate fluid flow. The effective implementation of RF-EMH for EEOR in an oil-bearing formation requires a RF power generator (RFG) capable of emitting high amplitudes and optimal phases. Such systems have been applied in Ion Cyclotron Resonance Heating (ICRH) systems using travelling waves [33], [34]. Transmission lines (TLs) convey power from the RFG to feed-points of antennas [35]. The transmission process becomes a primary source for power degradation due to impedance mismatches, radiation, and heat losses [36], [37]. Guided waves travelling along a TL reflect due to impedance variation in the transmission path. As such the effective design of the TL considers losses due to coupling mechanisms in the electromagnetic fields. Intrinsic parameters such as number of cables and their lengths are paramount in an antenna array scenario due to the number of feed-points required. Others include tubing permittivity, thermal and electrical conductivities and permeabilities of dielectrics [38].

A. ARTIFICIAL POWER LINE

The term artificial power line (APL) is introduced to distinguish signal level transmission from low-to-medium voltage transmission. For the purposes of the RF-EMH, the APL is based on metamaterial (meta-conductors) circuits designed to maintain high wave amplitudes. The unique properties of LH metamaterials, verified by full-wave analysis are promising for a diversity of optical/microwave applications, such as new types of beam steerers, modulators, band-pass filters, superlenses, microwave components and antennas. However, the LH structures presented originally were impractical for microwave applications, because of their too lossy and too narrow bandwidth characteristics, and alternative theories are desirable to gain a deeper insight into their behavior. A method to design an artificial left-handed transmission line (LH-TL) in the form of a lumped-elements ladder network has been described. It has been demonstrated that with ideal components, left-handedness can be achieved without losses over an unlimited bandwidth, starting from the cut-off frequency of the resulting high-pass filter and extending to infinity [38], [39]. This paper is organized as such; section II presents a conceptual open-hole barefoot well completion method consisting of an artificial power line placed between the tubing and casing walls. Section III presents a 2D axial model of power delivery system consisting of a conventional TL (RH-TL) right-handed medium is simulated to establish the thermal response of the well tubulars (steel tubing and casing). The electromagnetic coupling of the well tubulars to the TL is investigated. Section IV presents the lumped element method used to achieve the left-handedness of the TL model. The parameters of the APL are determined over the industrial heating frequency band (IHRFB). The results are presented and discussed in sections IV and V respectively.

B. CONCEPTUAL WELL STRUCTURE FOR RF-EMH

Steam injection has been extensively developed as a fundamental thermal recovery method [40]. This provides a framework for the design of EEOR well structures for enhanced performance. As a result, the proposed topology leverages existing well structures with modifications to accommodate power delivery. Wellbore tubulars define the pathway within which EM energy flows. Energy flow is described by the coupling of power transmission and heat transfer processes as shown in Figure 1(a).

C. DESCRIPTION OF PROPOSED STRUCTURE

Power generated by the RFG is transmitted via the coaxial TLs to the RF-EMH equipment (antenna array) at the bottom of the well. The antenna converts the power into thermal energy by propagating the waves to the formation. Figure 1 (a) presents the flow of power and subsequent radiation to reservoir pay-zone.

1) VERTICAL WELL STRUCTURE

The vertical well structure consists of long cylindrical steel tubing and casings as presented in Figure 1(b). The figure presents an axial-symmetric coordinate system (r, z) representation of the well tubulars over the well radius R_w and depth Z_w. The r-coordinate begins at the center of the air-filled tubing r_c towards its inner wall corresponding to $r_c < R_w < R_{ti}$, the second layer is the thickness of the tubing $R_{ti} < R_w < R_{to}$; the third layer is the annulus which extends to accommodate the APL as $R_{to} < R_w < R_{ci}$; the fourth layer represents the TL placed with a center at $R_w = r_0$ and covers $R_o < R_w < R_i$; the final layer before the cement layer is the production casing thickness defined as $R_{ci} < R_w < R_{co}$. The sizes of the tubing and casing are determined by consideration of the fluid produced - heavy oil.

2) TUBING AND CASING SIZES

The standard casing and tubing sizes in a vertical well producing from both saturated and undersaturated oil reservoirs are presented in 10 and 11 respectively. A predictive model determined the optimal tubing size (OTS) of 73 mm preferable in both cases [41]. The corresponding optimal casing size (OCS) was determined to be 139.7 mm [42]. At the bottom

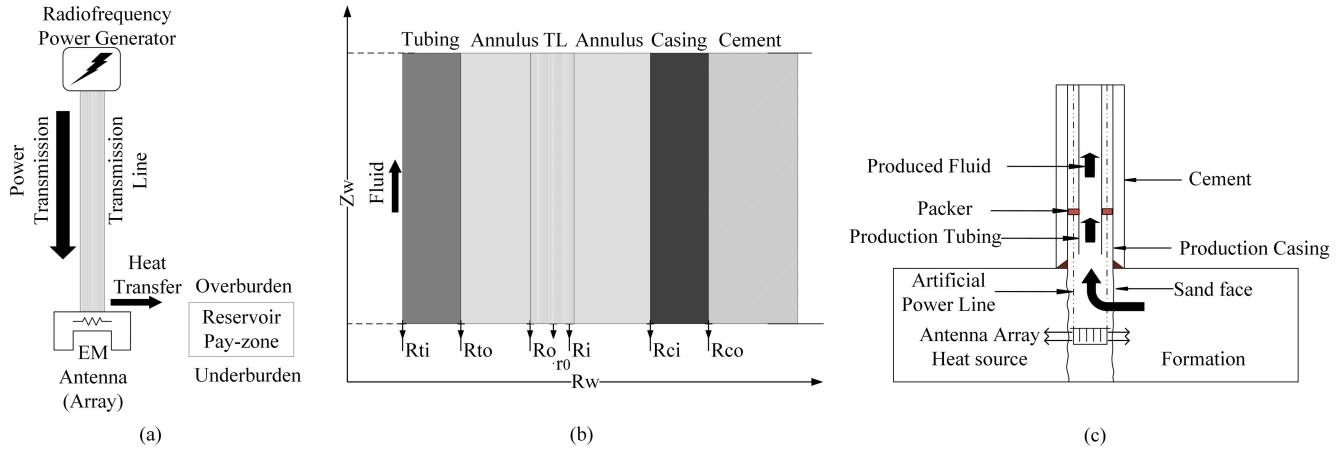

FIGURE 1. Proposed Well structure for RF-EMH. (a) Schematic diagram of power flow and energy transfer in downhole RF-EMH. (b) Wellbore tubular structure showing various components (c) Open-hole barefoot well completion with APLs feeding Antenna Array.

of the well (pay-zone layer), the antenna is fed by the APL suspended from the surface. At this point, it is preferable that EM waves are not reflected by obstructing surfaces.In order to protect RF heating equipment from sand accumulation, cased and perforated well completion method has been considered. While the method offers protection of RF antenna, it exposes the radiated waves to the reflective surface of the casing and obstructs wave propagation [43]. As such, the open-hole completion method was selected as shown in Figure 1(c).

II. RADIOFREQUENCY ENERGY TRANSMISSION IN WELL TUBULARS

Assuming an ideal RFG, voltages and currents are defined by the governing equations. Mechanisms of energy losses are defined and a lossless power transmission scenario is conceptualised over the designed frequency range. Because the application defines a need for flexibility due to sequential heating where energy may be temporarily shut off or directivity is required to specific regions of the pay-zone layer, the power parameters are focused on the effective IHRFB.

A. RF POWER TRANSMISSION FOR RADIOFREQUENCY ELECTROMAGNETIC HEATING

The RF power transmission model is governed by a modified telegrapher's equation due to the coupling of well tubulars to the coaxial RH-TL. Then, the tubular behaves like a parasitic coaxial transmission line excited from its dielectric substrate. In the coaxial RH-TL, assuming uniformity in propagation, a RH-TL is characterized by the phase constant β (or by the electrical length βl), and by the characteristic impedance, Z_o. In long TLs with traveling waves generated by a source, the characteristic impedance expresses the relation between voltage and current at any transverse plane of the line. Neglecting losses, the power carried by the traveling wave along the line is given by:

$$P^+ = \frac{I\left|V_o^+\right|^2}{2\,Z_o} \tag{1}$$

In electromagnetic heating, the TL is loaded by RF antenna or array. Consequently, the three different situations that arise are complete absorption, complete reflection and partial absorption and reflection A.38 to A.43. Assuming the load impedance Z_L, situated in the plane $z = 0$ (end of the line) with a line voltage wave of the form $V^+(z) = V_o^+ e^{-j\beta z}$, then the ratio of voltage to current for the wave is:

$$V^+(z)/I^+(z) = Z_o \tag{2}$$

At $z = 0$, the relation between the voltage, V_L, and the load current, I_L, satisfies Ohm's law as $V_L/I_L = Z_L$. Since, in general, $Z_L \neq Z_o$, a reflected wave must be generated at $z = 0$, such that Ohm's law is preserved. Hence, line voltage and current are expressed as:

$$V(z) = V_o^+ e^{-j\beta z} + V_o^- e^{j\beta z} \tag{3}$$

$$I(z) = \frac{V_o^+}{Z_o} e^{-j\beta z} - \frac{V_o^-}{Z_o} e^{j\beta z} \tag{4}$$

As such, Ohm's law at $z = 0$, yields:

$$Z_L = \frac{V(0)}{I(0)} = \frac{V_o^+ + V_o^-}{V_o^+ - V_o^-} Z_o \tag{5}$$

and the relation between the amplitude of reflected and incident wave, also known as reflection coefficient, is:

$$\rho_L = \frac{V_o^-}{V_o^+} = \frac{Z_L - Z_o}{Z_L + Z_o} \tag{6}$$

it follows that if $Z_L = Z_o$(matched load), $\rho_L = 0$ and the incident power is absorbed by the load (i.e., no reflections in the load). Conversely, if the load is an open or a short circuit, the reflection coefficient is $\rho_L(Z_L = \infty) = 1$ and $\rho_L(Z_L = 0) = -1$, respectively, and the incident power is reflected to the source. Where loads are fully reactive as: $|\rho_L(Z_L = j\chi)| = 1$, with χ as the reactance, incident power is reflected to the source. Although wave reflection in a TL is caused by a mismatch between the line and the load, and hence it is ultimately generated at the plane of the load ($z = 0$), the reflection coefficient can be generalized to

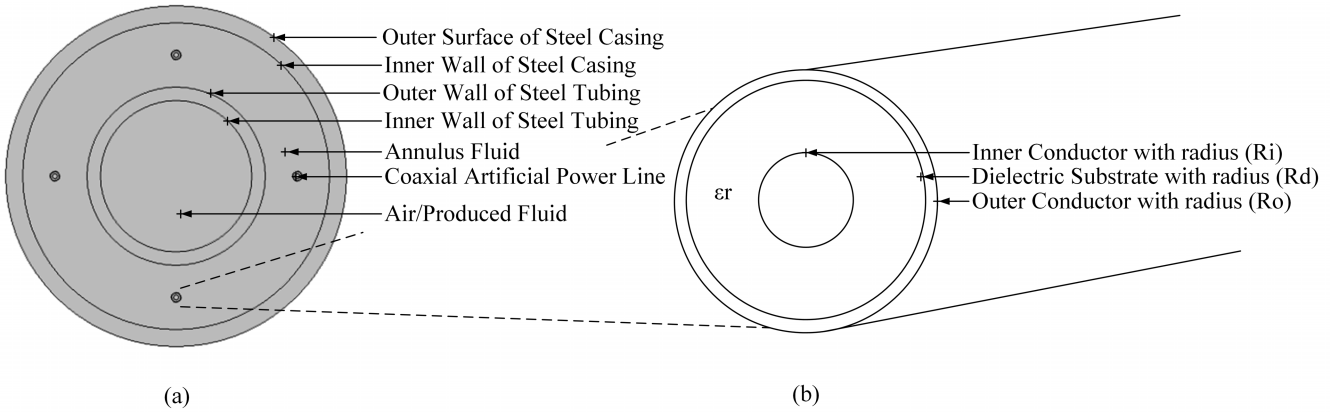

FIGURE 2. Power Transmission in well tubulars (a) Geometrical well tubular model for a 4-element uniform circular antenna array (b) Coaxial RH-TL model.

any plane of the line, as the ratio between the voltage of the incident and reflected wave, that is:

$$\rho(z) = \frac{V^-}{V^+} = \frac{V_o^- e^{j\beta z}}{V_o^+ e^{-j\beta z}} = \rho_L e^{2j\beta z} \tag{7}$$

where as expected,

$$|\rho(z)| = |\rho_L| \tag{8}$$

Practically, the assumption of a power supply with complex impedance, Z_s, is valid due to harmonics introduced from conversions and imperfect filtering. Such power is characterized by the wave reflection coefficient, s given by:

$$s = \frac{Z_{in} - Z_s^*}{Z_{in} + Z_s} \tag{9}$$

where the asterisk denotes complex conjugate, and Z_{in} is the impedance seen from the input port of the line. Then, the power transmission coefficient, which is relevant for power transmitted to the line for the general situation of a source with complex impedance, is given by:

$$\tau = 1 - |s|^2 = 1 - \left|\frac{Z_{in} - Z_s^*}{Z_{in} + Z_s}\right|^2 \tag{10}$$

The input impedance Z_{in}, which depends on the distance between the load and the input port can be simply computed as follows:

$$Z_{in} = \frac{V(-l)}{I(-l)} = \frac{V_o^+\left(e^{j\beta l} + \rho_L e^{-j\beta l}\right)}{V_o^+\left(e^{j\beta l} - \rho_L e^{-j\beta l}\right)} Z_o \tag{11}$$

The resulting equivalent electric circuit showing an antenna as the load is presented in Figure 3.

B. COAXIAL RIGHT-HANDED TRANSMISSION LINE WAVE PROPAGATION MODEL

In terms of wave propagation, the coaxial RH-TL presented in Figure 4 is a Sommerfeld-Goubau wire defined by an inner conducting wire coated with a sheet of low-loss dielectric material suitable for wave propagation [44]. The axial fields

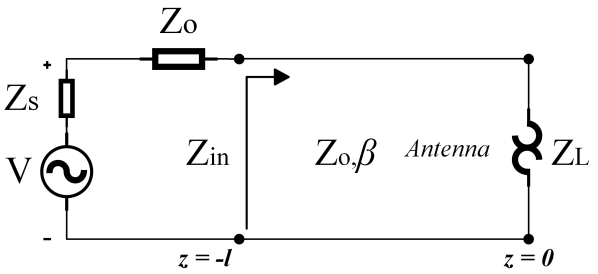

FIGURE 3. Equivalent electric circuit representation of a voltage excited transmission line for RF-EMH.

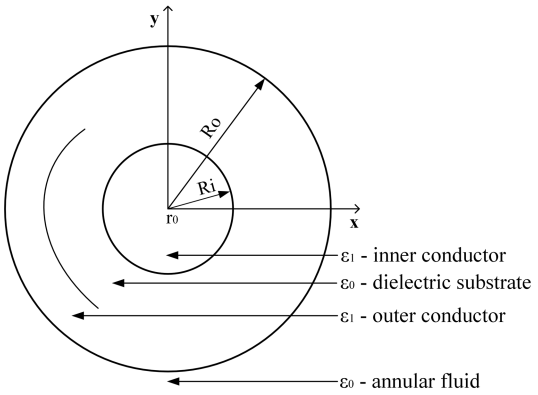

FIGURE 4. 2D cartesian geometry of the Sommerfeld-Goubau coaxial TL.

within the dielectric substrate of the coaxial RH-TL are given by:

$$E_z^{(1)}(r,\theta) = \sum_{n=-\infty}^{\infty} [A_n^{(1)} J_n(p_1 r) + A_n^{(2)} Y_n(p_1 r)] e^{jn\theta} \tag{12}$$

$$H_z^{(1)}(r,\theta) = \sum_{n=-\infty}^{\infty} [B_n^{(1)} J_n(p_1 r) + B_n^{(2)} Y_n(p_1 r)] \tag{13}$$

where $A_n^{(1)}$, $A_n^{(2)}$, $B_n^{(1)}$ and $B_n^{(2)}$ are arbitrary constants. Then, the axial fields in the annular fluid region are given by:

$$E_z^{(0)}(r,\theta) = \sum_{n=-\infty}^{\infty} C_n K_n(q_0 r) e^{jn\theta} \tag{14}$$

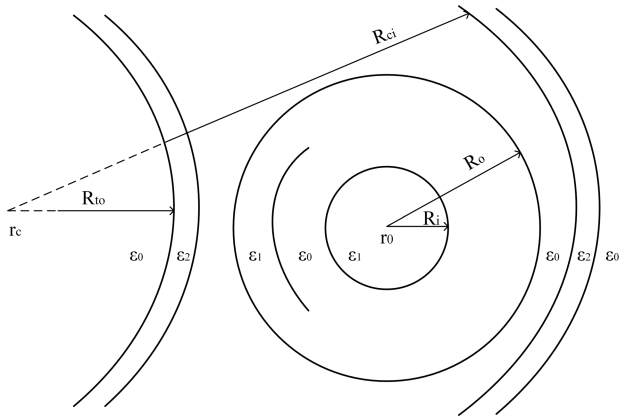

FIGURE 5. 2D geometry of well tubular as a hollow concentric cylindrical dielectric waveguide with coaxial TL (geometry not to scale).

$$E_z^{(0)}(r,\theta) = \sum_{n=-\infty}^{\infty} C_n K_n(q_0 r)\, e^{jn\theta} \tag{15}$$

where C_n, D_n are arbitrary constants.

C. WELL TUBULARS AS A CONCENTRIC CYLINDRICAL HOLLOW WAVEGUIDE

When the RH-TL is placed between the outer tubing and the inner casing walls with finite conductivities, the tubular structure acts as a hollow concentric cylindrical dielectric waveguide in the presence of RF excitation as presented in Figure 5. Under these circumstances, the position of the TL within the tubular space influences the EM field distribution. The annular fluid of permittivity ε_0 is surrounded by a concentric layer of dielectric material having dielectric constant ε_2. The conditions defining the concentric cylindrical hollow tubular waveguide is presented in Table 1. The concentric cylindrical hollow waveguide consists of a dielectric domain ($R_{to} \leq R_w \leq R_{ci}$) terminated at its ends by reflecting tubular walls that are perpendicular to the axis of the RH-TL. For a circular step-index TL, the HE_{11} mode is the dominant mode for the well tubular waveguide. Electromagnetic energy is introduced into the tubulars via the coaxial RH-TL positioned at $R_w = r_0$. At resonance, the diameter of the hollow cavity defined by ($R_{to} \leq R_w \leq R_{ci}$) must be $n\lambda_g/2$ (n an integer), where λ_g is the guide wavelength of the particular mode under consideration. By measuring the resonant frequencies of the cavity, one may obtain the guide wavelength of that mode in the dielectric waveguide. The propagation constant, β, of that mode is related to λ_g and v_p, the phase velocity, as follows:

$$\beta = \frac{2\pi}{\lambda_g} = \frac{\omega}{v_p} \tag{16}$$

D. POWER DISSIPATION AND ENERGY LOSSES

It is assumed that the EM waves travelling along the TL lose part of their energy, which creates internal distributed heat sources in the tubing and casing walls [45]. While the heat generated along the power lines introduce the primary heat source, the coupling due to EM fields along the metallic tubular surfaces create secondary heat sources in tubing and casing. Heating of well tubulars may be an advantage in fluid flow conditions. In thermal recovery methods, the temperature dependent viscosity of produced fluid becomes threatened by low temperature surfaces. This leads to the glass transition phase depicted by increase in oil viscosity and relaxation time [46]. This paradox of power transmission efficiency and thermal losses further emphasizes the need for control over thermal response of tubulars. Transmission losses are primarily due to finite conductivity of the metals (conductor losses), dissipation in the dielectric, and radiation. Depending on load conditions, radiation losses may dominate the losses, therefore, TLs carrying travelling waves must be designed to minimize radiation losses [47]. The Q of the tubular structure indicates the energy storage capacity of a structure relative to the associated energy dissipation from various loss mechanisms, such as those due to the imperfection of the dielectric material and the finite conductivity of tubular surfaces [44]. The common definition of Q is applicable to the TL and is given by:

$$Q_{TL} = \frac{\omega \bar{W}_{TL}}{\bar{P}_{TL}} \tag{17}$$

where ω is the angular frequency, $\bar{W}_{TL}$ is the total time average stored energy in the TL, and $\bar{P}_{TL}$ is the time average power dissipation of the TL. With a well designed coaxial RH-TL and accurate r_0 position, the time average power dissipation of the tubular structure $\bar{P}$ consists of two parts, the power loss due to the TL and that due to the tubular walls, namely,

$$\bar{P} = \bar{P}_{TL} + \bar{P}_{tubular} \tag{18}$$

The power dissipation due to the TL is given by:

$$\bar{P}_{TL} = \frac{1}{2}\sigma_{TL} \int_0^{TL} \int_{A_{TL}} \left(E_1 \cdot E_1^*\right)\, dA\, dz \tag{19}$$

where E_1 is the electric field within the TL, σ_{TL} is the conductivity of the TL, A_{TL} is the cross-sectional area of the TL, and the asterisk denotes the complex conjugate. The ohmic losses at both tubular walls are given by:

$$\bar{P}_{tubular} = 2\left(\frac{R_s}{2}\right) \int_{A_w} \left(H_t \cdot H_t^*\right)\, dA \tag{20}$$

where $R_s = \sqrt{\frac{\omega\mu}{2\sigma_r}}$, the tubular resistivity; σ_r is the conductivity of the steel tubing and casing, and H_t is the tangential component of the magnetic field along the tubular surface. Here, A_w is the area of the conducting tubing/casing, outside of which the electromagnetic fields are neglected. The time average energy stored is given by:

$$\bar{W} = 2\bar{W}_m = \mu_0 \int_V \left(H \cdot H^*\right)\, dV \tag{21}$$

where V is the volume of the cavity, $\bar{W}_m$ is the time average magnetic field energy, and H is the total field.

TABLE 1. Boundary conditions of concentric cylindrical hollow tubular waveguide.

Region	RH-TL	Tubular cavity	Beyond cavity
$r-axis$	$(r_0 \leq R_i \leq R_o)$	$(R_{to} \leq R_w \leq R_{ci})$	$(r \leq R_w \leq R_{to}$ and $R_{ci} \leq R_w \leq r)$
Electric field	$E_z^{(1)} = C_1 J_n(p_1 r)$	$E_z^{(2)} = C_2 J_n(p_2 r) + C_2{'} Y_n(p_2 r)$	$E_z^{(3)} = G K_n(qr)$
Magnetic field	$H_z^{(1)} = D_1 J_n(p_1 r)$	$H_z^{(2)} = D_2 J_n(p_2 r) + D_2{'} Y_n(p_2 r)$	$H_z^{(3)} = F K_n(qr)$
	${p_1}^2 = \omega^2 \mu_0 \epsilon_0 - \beta^2$	${p_2}^2 = \omega^2 \mu_0 \epsilon_2 - \beta^2$	$q^2 = \beta^2 - \omega^2 \mu_0 \epsilon_0$

E. TELEGRAPHER's EQUATION AND LUMPED ELEMENT APPROACH

Conventional TLs are denoted as right-handed (RH) media due to positive permeability and permittivity values. In ordinary (RH) media, waves decay as they propagate since the energy is lost by mechanisms stated. Meanwhile, waves grow in the direction of propagation of the wavefronts in left-handed (LH) media. This result can be obtained, by considering that the real part of the permeability and permittivity are negative, as corresponds to LH media, whilst the imaginary parts are both negative, as results from the well-known complex Poynting theorem and energy conservation considerations [47]. By considering a plane wave with square wave number:

$$k^2 = \omega^2 \varepsilon \mu \tag{22}$$

it can be deduced that $Im\left(k^2\right) > 0$ in LH media. This can be shown by expressing k, ε and μ as:

$$k = k' + jk'' \tag{23}$$

$$\varepsilon = \varepsilon' + j\varepsilon'' \tag{24}$$

$$\mu = \mu' + j\mu'' \tag{25}$$

where the explicit negative sign in the imaginary part of ε and μ has been considered, namely, $Im\,(\varepsilon) = -\varepsilon''$ and $Im\,(\mu) = -\mu''$, ε'' and μ'' being positive quantities. Introducing (23) into (24), we obtain the following:

$$k'^2 - k''^2 + 2jk'k'' = \omega^2 \left[\mu'\varepsilon' - \mu''\varepsilon'' - j\left(\mu'\varepsilon'' + \varepsilon'\mu''\right)\right] \tag{26}$$

From which it follows that: $\mathrm{Im}(k^2) = 2k'k'' > 0$ if ε' and μ' are negative. Finally, if $\mathrm{Im}(k^2) > 0$, then its either $\mathrm{Re}(k) > 0$ and $\mathrm{Im}(k) > 0$ or $\mathrm{Re}(k) < 0$ and $\mathrm{Im}(k) < 0$.

1) MINIMIZING TRANSMISSION LINE LOSS

To design a low-loss TL, the phase constant and the characteristic impedance can be closely approximated by considering the line as lossless. While a linear approximation of the phase constant is valid in low-loss lines, over large lengths of the TL, dispersion may occur leading to energy distortion. To simplify the approximation, the lumped element method was considered above the distributed element method. For the distributed element method, where nonuniformity is assumed for the voltages and currents along constituent circuit elements, the accuracy obtained is not worth the complexity. Whereas, the lumped element method assumes that the voltages and currents in the line are uniform and independent on the line progression. This approach is valid for frequencies

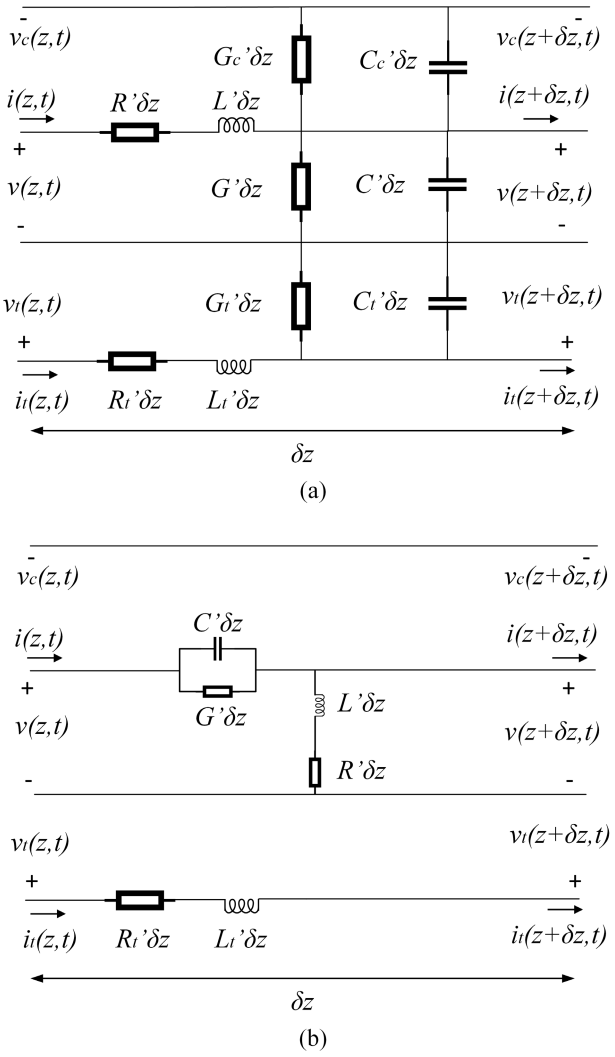

FIGURE 6. Lumped element equivalent circuit of (a) RH-TL with mutual coupling along tubing and casing surfaces (b) derived LH-TL without coupling.

below 100 MHz which accommodates the IHRFB. As such, the voltages and currents are dictated by the Kirchhoff's current and voltage laws and by the terminal equations of the lumped elements present along the line [47]. The coaxial TL is described by cascading the lumped element two-port network unit cell depicted corresponding to an infinitesimal piece of the power line. Corresponding line parameters are denoted by δz length while C', L', R', and G' are the line capacitance, line inductance, line resistance, and line conductance per unit length, respectively. R' is related to conductor losses, whereas G' accounts for dielectric losses. From

Kirchhoff's circuit laws applied to the network of Figure 6 the following equations are obtained:

$$v(z,t) - R'\delta z \cdot i(z,t) - L'\delta z \frac{\partial i(z,t)}{\partial t} - v(z+\delta z,t) = 0 \quad (27)$$

$$i(z,t) - G'\delta z \cdot v(z+\delta z,t) - C'\delta z \frac{\partial v(z+\delta z,t)}{\partial t} - i(z+\delta z,t) = 0 \quad (28)$$

similarly, resulting parasitic coupling is described by introducing the steel tubing/casing separated from the coaxial TL by a dielectric substrate and its unit cell circuit as shown in Figure 7. The induced tubing voltage and tubing currents are presented as:

$$v_t(z,t) - R'_t\delta z \cdot i_t(z,t) - L'_t\delta z \frac{\partial i_t(z,t)}{\partial t} - v_t(z+\delta z,t) = 0 \quad (29)$$

$$i_t(z,t) - G'_t\delta z \cdot v_t(z+\delta z,t) - C'_t\delta z \frac{\partial v_t(z+\delta z,\ t)}{\partial t} - i_t(z+\delta z,t) = 0 \quad (30)$$

with subscript "t" representing parasitic parameters of tubing/casing. The resulting frequency dependent wave characteristics from the adopted lumped approach is given by:

$$\gamma(\omega) = \alpha(\omega) + j\beta(\omega) = \sqrt{Z'Y'} = \sqrt{(G'+j\omega C')^{-1}(R'+j\omega L')^{-1}} \quad (31)$$

where $\alpha(\omega)$ is the attenuation factor and $\beta(\omega)$ is the propagation factor. Furthermore, the identical characteristic impedance of the line is given as:

$$Z_c(\omega) = \sqrt{Z'/Y'} = \sqrt{\frac{R'+j\omega L'}{G'+j\omega C'}} \quad (32)$$

In a lossless scenario, the attenuation factor becomes $\alpha = 0$, due to $G' = R' = 0$, then

$$\beta(\omega) = -\frac{1}{\omega\sqrt{L'C'}} \quad (33)$$

The superluminal propagation and dispersion parameters of the proposed medium have been effectively resolved [48].

2) LEFT-HANDED TRANSMISSION LINE

Practically, purely left-handed structures are not possible to obtain due to the presence of reactive currents and voltages which occur as a wave propagates along the left-handed structures. The capacitor current induces magnetic fluxes leading to a series inductance. Meanwhile the shunt inductance is influenced by the capacitance between the stubs. These induced reactances create internal resonances within the left-handed reactances. This leads to right-handed characteristics within the left-handed material. At this point, to achieve the desired left-handedness, the balance of resonances between the induced reactances is necessary. When the balance is achieved, the left-handed transmission line becomes frequency independent and can transmit RF waves over an unlimited bandwidth. Using the lumped element approach, the LH-TL can be achieved over large depths required for downhole RF-EMH, unit cells in series create a ladder network as seen in Figure 7. This approximation is described and characterized by length and times unit length parameters as in Figure 7(a), it suffices to repeat the unit cell shown in Figure 7(b) into the ladder network configuration represented in Figure 7(c), with unit cell components values represented by:

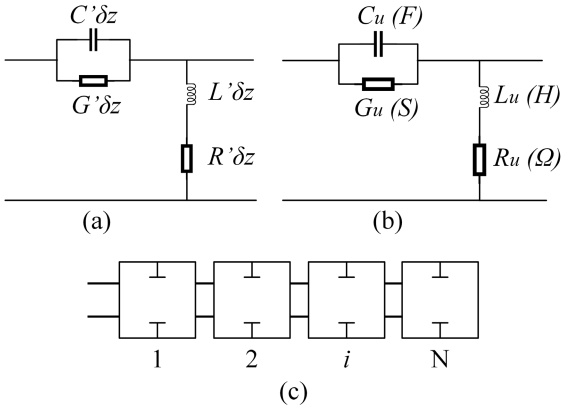

FIGURE 7. Electrical representation of lumped unit cell (a) Unit circuit cell of lumped APL ladder network (b) Unit immittances of APL cell (c) APL equivalent obtained by cascading N unit cells.

$$K_u = K'\delta z = K'\left(\frac{N}{z}\right) \quad (34)$$

where K is a generic variable for C, L, G, R, N is the number of cells and $\delta z = z/N$ is the approximated cell unit length. Realistically, the minimum number of stages required to have a sufficiently accurate approximation of the line at a given frequency f_0 is estimated by $\delta z < \lambda/5$ obtained from:

$$N > \frac{5\delta z}{(2\pi)^2\sqrt{L'C'}f_0} \quad (35)$$

With this condition, the electrical length of the unit cell is small enough to be a lumped element and the practical implementation of the line is a translation of the ideal lumped element line into a cascaded form. To evaluate the expression over large depths of the TL, we consider the limit case where the number of stages with arbitrary immitances (series impedances and admittances) is infinite, where the input impedance at each stage is equal to that of the next stage. Then, $Z_{in}^{\infty} = Z + [(1/Y) \,||\, Z_{in}^{\infty}]$ so that $Z_{in}^{\infty} = Z/2 \cdot \left[1 \pm \sqrt{1 + 4/(YZ)}\right]$. Substituting the immittances values for a lossless TL yields the input impedance as:

$$Z_{in}^{\infty} = -\frac{j}{2\omega C_u}[1 + j\sqrt{4\omega^2 L_u C_u - 1}] \quad (36)$$

At sufficiently high frequencies, Z_{in}^{∞} exhibits a real component which is equal to the characteristic impedance of the fictitious line to approximate, according to (41) and shows that matching to ports with impedance Z_0 will be achieved by choosing $Z_0 = \sqrt{\frac{L_u}{C_u}}$. As frequency decreases, the magnitude

of the term under the radical sign eventually becomes zero. At and below this frequency, Z_{in}^{∞} is purely imaginary, and no power can be delivered to the line. The cut-off frequency is therefore given by:

$$f_c^{N\to\infty} = \frac{1}{4\pi\sqrt{L_u C_u}} \tag{37}$$

III. SIMULATION

In various schemes of thermal recovery of heavy oil, a pre-treatment phase is often established before production. This is usually determined by pre-production reservoir assessments. Based on this, the models considered pre-operational conditions where the production of heavy oil is yet to commence. The assumptions are made for standard atmospheric conditions and transient parameters are not considered.

A. MODELLING ASSUMPTIONS

To establish a standard benchmark for performance and for future comparative analysis, material properties were assumed to be linear, homogeneous and isotropic. The coaxial RH-TL is made of copper material with properties presented in Table 4. The annulus domain and the inner region of the tubing are assumed to have equal dielectric permittivity. The tubing and casing are made of the same steel material with different thickness as presented in Table 4. The cement region beyond the outer casing layer was neglected.

B. SOLUTION METHODOLOGY

The models developed were computed using a finite element commercial simulation software COMSOL. The methodology follows a finite element discretization which leads to a linearized eigenvalue problem. In non-linear cases, COMSOL assembles quadratic approximations to achieve linearization and convergence. The solution flowchart is presented in Figure 8. The RF electromagnetic waves module was used within the modeling interface. A frequency domain study was initiated with modal analysis to evaluate the wave propagation characteristics of the model. Then a frequency parametric sweep was conducted over the IHRFB. In the RH-TL conductors, relative permeability magnetization model was assumed and conduction was governed by the electrical conductivity of the material. In order to identify the mechanisms of coupling, air was assumed as TL dielectric substrate material and annular fluid to allow the determination of EM field distribution within the modeling domain. This assumption is consistent with practical air-filled transmission lines [49], [50], [51].

C. MODE ANALYSIS

1) EIGENVALUE SEARCH METHOD

In order to determine the resonance modes during RF-EM wave transmission, an eigenvalue solver algorithm is used. The eigenvalue region method uses an algorithm based on Arnoldi Package (ARPACK) algorithm for solving eigenvalue problems. This enables finding all eigenvalues within a small rectangular region in the complex plane. The algorithm uses ARPACK to find eigenvalues covering a rectangle in the complex plane containing the sought eigenvalues; that is, there are eigenvalues with real or imaginary parts larger and smaller than the given smallest and largest real or imaginary parts. The algorithm uses four numbers defining a rectangle in the complex plane i.e. the largest real number, smallest real number, largest imaginary number, and smallest imaginary number. When the largest and smallest real or imaginary numbers are equal, the algorithm considers only an interval on the real or imaginary axis, respectively. An approximate number of eigenvalues. The maximum number of eigenvalues. The shift is taken as the center of the rectangle of sought eigenvalues. In COMSOL, the ARPACK mode solver was used with varying number of desired modes. The solver searches for eigenvalues closest to the shift σ. This computes the largest eigenvalues and to minimize the instances of symmetric modes, the desired number of modes were limited to 6 to reveal active resonance.

TABLE 2. Table of computational parameters.

Description	Value	
Sweep type	All combinations	
Parameter	**Value list**	**unit**
f_0	5, 13.56, 27.12, 54.24	MHz
r_0	0.04, 0.049685, 0.058	m

TABLE 3. Table of study parameters.

Parameter	Value	Unit
Transform	EMI	#
Analysis frequency	f_0	MHz
Solver type	ARPACK	#
Desired number of modes	6	#
Shift search parameter	absolute value	

D. COAXIAL RIGHT-HANDED TRANSMISSION LINE MODEL

The coaxial RH-TL model was developed by defining the geometrical parameters and assigning the dimensions based on the coaxial cable optimal power transfer ratio of outer conductor to inner conductor diameter of 1.65. Based on the geometrical model presented in Figure 9(a), a 2D symmetric model was developed to evaluate the response of a RH-TL in the well tubulars and evaluate its left-handedness over the IHRFB. The resulting computational model is presented in Figure 9(b).

E. WELL TUBULAR WAVEGUIDE MODEL

The well tubular model consists of the coaxial RH-TL sub-model earlier developed for the evaluation of its characteristic impedance over the IHRFB. Subsequently, a 4-element array scenario was considered. The dimensions used are presented in Table 4.

IV. RESULTS

The results obtained from the computations of the sub-model of the coaxial RH-TL and the resulting model of the well

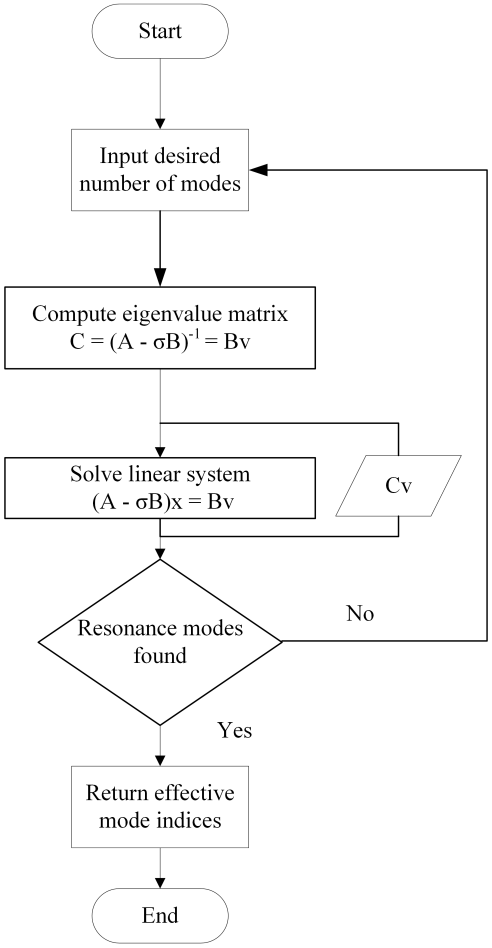

FIGURE 8. Resonance mode identification flowchart using ARPACK solver in COMSOL.

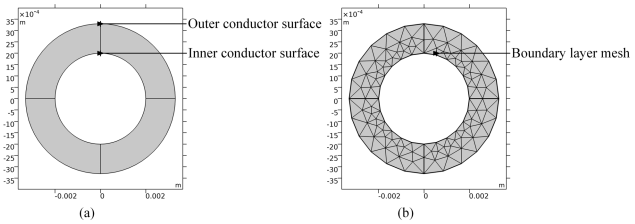

FIGURE 9. 2D computational model of coaxial RH-TL (a) 2D geometrical model of coaxial RH-TL (b) Meshed 2D computational model of coaxial RH-TL (complete mesh consists of 1855 domain elements and 232 boundary elements).

tubular waveguide are presented in the following subsections. Firstly, the frequency dependent characteristics of the coaxial RH-TL which determine the response of the well tubular model are presented. Consequently, the modal analysis of the waveguide model is performed.

A. EVALUATION OF RIGHT-HANDED TRANSMISSION LINE CHARACTERISTICS OVER IHRFB

To evaluate the impedance of the RH-TL, the model was computed for four values of f_0 at near vacuum effective mode indices. The results are presented in Figure 10(a) to (d).

TABLE 4. Well tubular waveguide model parameters.

Parameter	Value - Unit	Description
f_0	$5e6$–$60e6$ Hz	Operational frequency range
R_{co}	139.7/2 mm	Radius casing outer
R_{ci}	$R_{co} - \delta R_c$ mm	Radius casing inner
R_{to}	73/2 mm	Radius tubing outer
R_{ti}	$R_{to} - \delta R_t$ mm	Radius tubing inner
δR_t	11 mm	Thickness of tubing
δR_c	6.98 mm	Thickness of casing
R_o	3.3 mm	Radius outer conductor
R_i	2 mm	Radius inner conductor
r_0	$R_{to} + (R_{ci} - R_{to})/2$	Midpoint of transmission line

TABLE 5. Model material properties.

Material	Parameter	Value	Unit
Air	Relative permeability	1	1
	Relative permittivity	1	1
	Electrical conductivity	0	S/m
	Ratio of specific heats	1.4	1
	Refractive index, real part	1	1
	Refractive index, imaginary part	0	1
Copper	Relative permeability	1	1
	Electrical conductivity	5.998e7	S/m
	Heat capacity at constant pressure	385	J/(kg·K)
	Relative permittivity	1	1
	Density	8960	kg/m³
	Thermal conductivity	400	W/(m·K)
	Coefficient of thermal expansion	17e-6	1/K
	Young's modulus	110e9	Pa
	Poisson's ratio	0.35	1
	Reference resistivity	1.72e-8	Ω·m
	Resistivity temperature coefficient	0.0039	1/K
	Reference temperature	298	K
Steel	Relative permeability	1	1
	Electrical conductivity	4.032e6	S/m
	Relative permittivity	1	1
	Heat capacity at constant pressure	475	J/(kg·K)
	Thermal conductivity	44.5	W/(m·K)
	Coefficient of thermal expansion	12.3e-6	1/K
	Density	7850	kg/m³
	Surface emissivity	0.8	1
	Young's modulus	200e9	Pa
	Poisson's ratio	0.30	1

With the current distribution evaluated, the resulting effect of frequency and effective mode on the characteristic impedance of the line was investigated with the values presented in Table 6.

B. MESH ANALYSIS

In order to evaluate the accuracy of the results, the model was computed using two level mesh refinement with various degrees of freedom. As an electromagnetic heating analysis problem, the differences obtained in the results are negligible in relation to the computational time. The mesh parameters are presented in Table 7.

C. MODE ANALYSIS OF COAXIAL RIGHT-HANDED TRANSMISSION LINE IN WELL TUBULARS

As mode analysis is an eigenfrequency study, it is sufficient to compute the model without sources. A perfect electrical conductor boundary is assigned to the external surface of the outer conductor as presented in Figure 9(a) with the resulting mesh in Figure 9(b).

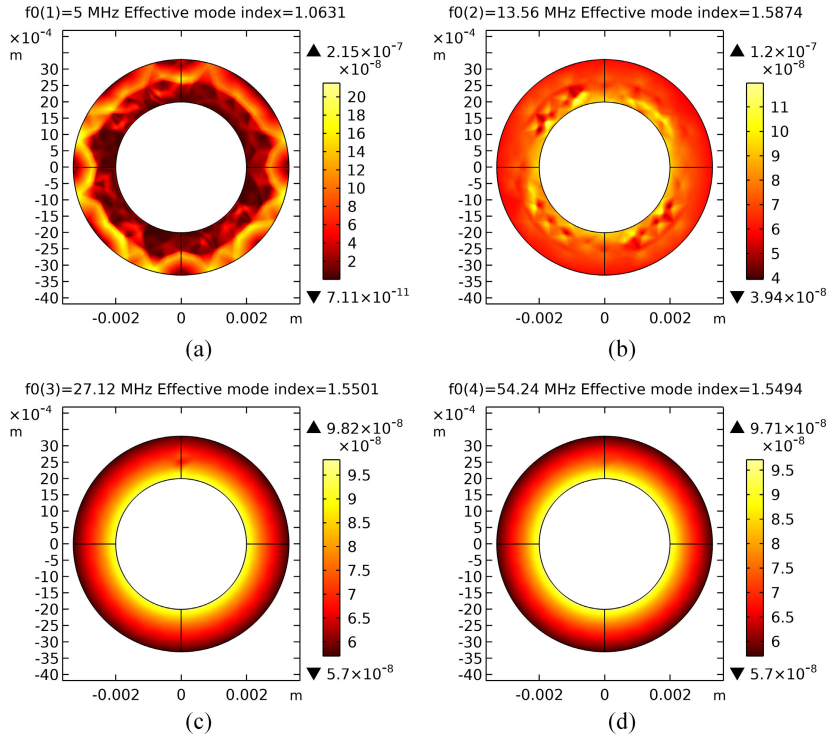

FIGURE 10. Current distribution along the surfaces of the coaxial RH-TL at effective modes indices near 1. (a) $f_0 = 5$ MHz with EMI =1.0631 (b) $f_0 = 13.56$ MHz with EMI =1.5874 (c) $f_0 = 27.12$ MHz with EMI =1.5501 (d) $f_0 = 54.24$ MHz with EMI =1.5494.

TABLE 6. Characteristic impedance of coaxial transmission line at near various effective mode indices.

f_0 [MHz]	Effective mode index - EMI	Characteristic impedance $[Z_c]$
5	1.0631398207126237 +4.026177566975599e-6i	28.344569252888338 -1.0734118697603836e-4i
13.56	1.5874013658015595 +3.351604870317951e-8i	18.983377005068192 -4.007616821082008e-7i
27.12	1.5500771818413823 +4.865382368337105e-9i	19.440476135181896 -6.099497823692648e-8i
54.24	1.5494271695256334 +3.117467457703393e-11i	19.448631758879692 -3.7748715237432075e-10i

TABLE 7. Mesh refinement parameters.

Refinement	Element type	NoE	DoF	Solution time
1	DE	1382	14279	58 s
	BE	209	9785	
			10569	
2	DE	8436	63503	233 s
	BE	548	58771	
			57469	

1) SINGLE COAXIAL RIGHT-HANDED TRANSMISSION LINE IN WELL TUBULAR

The first case considered for the well tubular waveguide model is when a single RH-TL is placed in the annular space between the surfaces of the tubing and casing. In this case, the tubular waveguide is excited from within its dielectric medium by a single TL. The resulting geometrical model developed is presented in Figure 11(a) and (c) with their mesh in Figure 11(b) and (d). With its r_0 position at the middle of the annular radius (neutral bias), the EM field distribution is evaluated as presented in Figure 12(a) to (h). For the single RH-TL in the well tubular, the effects of tubing and casing bias with regards to its position in the annular radius was evaluated for resonant modes and coupling intensity. The results for the tubing bias are presented in Figure 13(a), (c) and (e) whereas, Figure 13(b), (d) and (f) present the casing bias. The characteristics of the EM waves as transmitted along the TL were evaluated with emphasis on the attenuation and propagation constants over the IHRFB as presented in Figure 14(a). The total magnetic and electrical energy over the same range are presented in Figure 14(b). The effect of coupling due to neutral and biased positions on the power loss is presented in Figure 14(c).

2) 4-ELEMENT ARRAY OF UNIFORMLY SPACED RIGHT-HANDED TRANSMISSION LINES IN WELL TUBULARS

In order to achieve a model for the uniformly spaced 4-element array configuration, the geometrical and computational models presented in Figure 11(a) and (b) for the case of a single TL in the well tubulars were modified as shown in Figure 11(c). This was achieved by replicating the single RH-TL model and positioning it in the (x, y) cartesian plane at $(-r_0,0)$,$(0, r_0)$, and $(0, -r_0)$. The model was meshed as shown in Figure 11(d) and computed. Modal analysis at near vacuum effective mode index was performed for f_0 at 5 MHz, 13.56 MHz, 27.12 MHz and 54.24 MHz and presented in Figure 15(a) to (d) respectively.

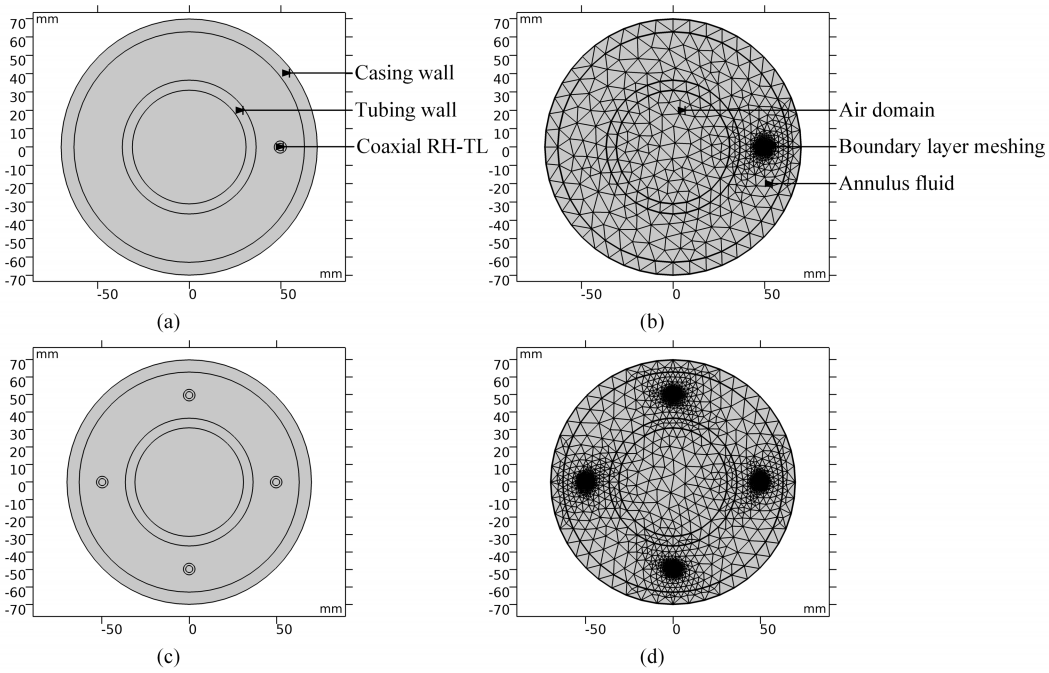

FIGURE 11. 2D model of well tubular waveguide (a) Well tubular with single RH-TL (b) Meshed model of well tubular with RH-TL showing boundary layer meshing of the coaxial RH-TL (c) Well tubular with 4-element uniform array of RH-TLs (d) Meshed model of well tubular with 4-element uniform array of RH-TLs.

D. LEFT-HANDED ARTIFICIAL POWER LINE DETERMINATION WITH IDEAL LUMPED ELEMENTS

Assuming a practical pay-zone depth of 10 m to 60 m, the z-axis depth of the TL is obtained. Conventional RH-TL characteristic impedance of 50 Ω also provides input for the evaluation of lossless parameters L_u and C_u. The frequency band is obtained from literature establishing the IHRFB of $5 - 60$ MHz [13], [14]. To establish a depth-to-frequency correlation based on the number of phases of the resulting APL, cut-off frequency is evaluated.

V. DISCUSSION

A. RF TRANSMISSION EFFICIENCY

The challenge of adopting RF-EM heating for the recovery of heavy oil has been characterised from an efficiency perspective. The efficiency of RF power generation by a RFG, transmission via TLs and propagation via antennas have defined the constituent components. However, a holistic approach to the enhancement of the method has been missing. This could be attributed to a focus on application of the waves rather than the mechanisms of their transmission and subsequent propagation. Wave transmission in a coaxial TL occurs in TEM (transverse electric and magnetic) mode. However, due to parasitic reactances defined by the capacitance between the conductive surfaces of well tubulars and the induction by their proximity to the EM fields, the tubulars demonstrate induced voltages and currents. The modes by which these parameters propagate are either TE (transverse electric) or TM (transverse magnetic). Because the reactances are frequency dependent, resonance modes are activated at arbitrary frequencies by their interaction with the fundamental transmission frequency. At resonance, energy losses are enhanced and transmission amplitudes are attenuated. With an efficient RFG, the overwhelming task becomes the transmission of optimal wave amplitudes over large depths for the enhancement of antenna input power. It has been established that antenna propagation frequencies determine the penetration depth of EM energy within reservoir pay-zones. By identifying the industrial heating radio-frequency band, the required antenna propagation frequencies are effectively streamlined.

B. EFFECT OF RESONANCE MODES IN EM COUPLING

RF power transmission has been associated with losses along the depths of vertical wells. By determining the propagation modes, the resonance frequencies of the EM waves were observed. The fields generated around the TL provided a pathway for energy transfer between TL and well tubulars. The progression of current flow near the surface of the inner conductor was observed within the IHRFB. With increase in the frequency from 5 MHz and 13.56 MHz in Figure 10(a) and (b), the current due to skin effect shields the inside of the conductor at 27.12 MHz and 54.24 MHz as seen in Figure 10(c) and (d). As a result, the complex characteristic impedance of the line decreased from $28.34 - 1.073e - 4i$ Ω at 5 MHz to $19.45 - 3.77e10i$ Ω at 54.24 MHz with increase in the frequency as seen in Table 5. This is due to the fact that resistance and inductance depend on the skin depth and are therefore only valid at frequencies where the skin depth is much smaller than the physical thickness of the conductor. As such, the inductance due to the penetration of the magnetic field into a metal of finite conductivity is negligible at sufficiently high frequencies. In the case of the concentric

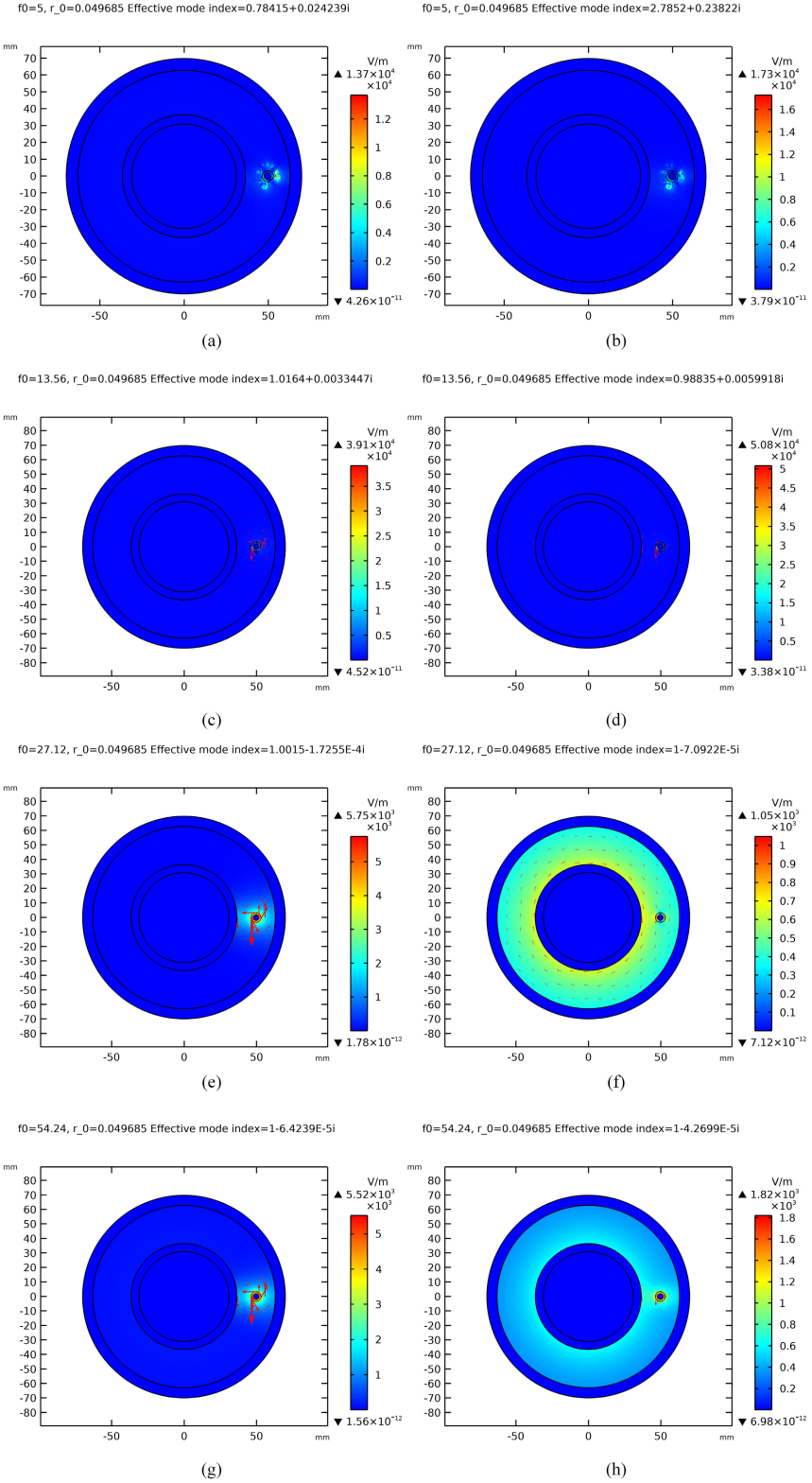

FIGURE 12. EM field distribution in well tubular with TL at $R_w = r_0 = 0.049685\ m$ (a) $f_0 = 5$ MHz with EMI $= 0.785 + 0.0242i$ (b) $f_0 = 5$ MHz with EMI $= 2.785 + 0.2382i$ (c) $f_0 = 13.56$ MHz with EMI $= 0.9883 + 0.0059i$ (d) $f_0 = 13.56$ MHz with EMI $= 1.016 + 0.003344i$ (e) $f_0 = 27.12$ MHz with EMI $= 1.0015 - 1.7255e-4i$ (f) $f_0 = 27.12$ MHz with EMI $= 1 - 7.09e-5i$ (g) $f_0 = 54.24$ MHz with EMI $= 1 - 6423e-5i$ (h) $f_0 = 54.24$ MHz with EMI $= 1 - 4.269e-5i$.

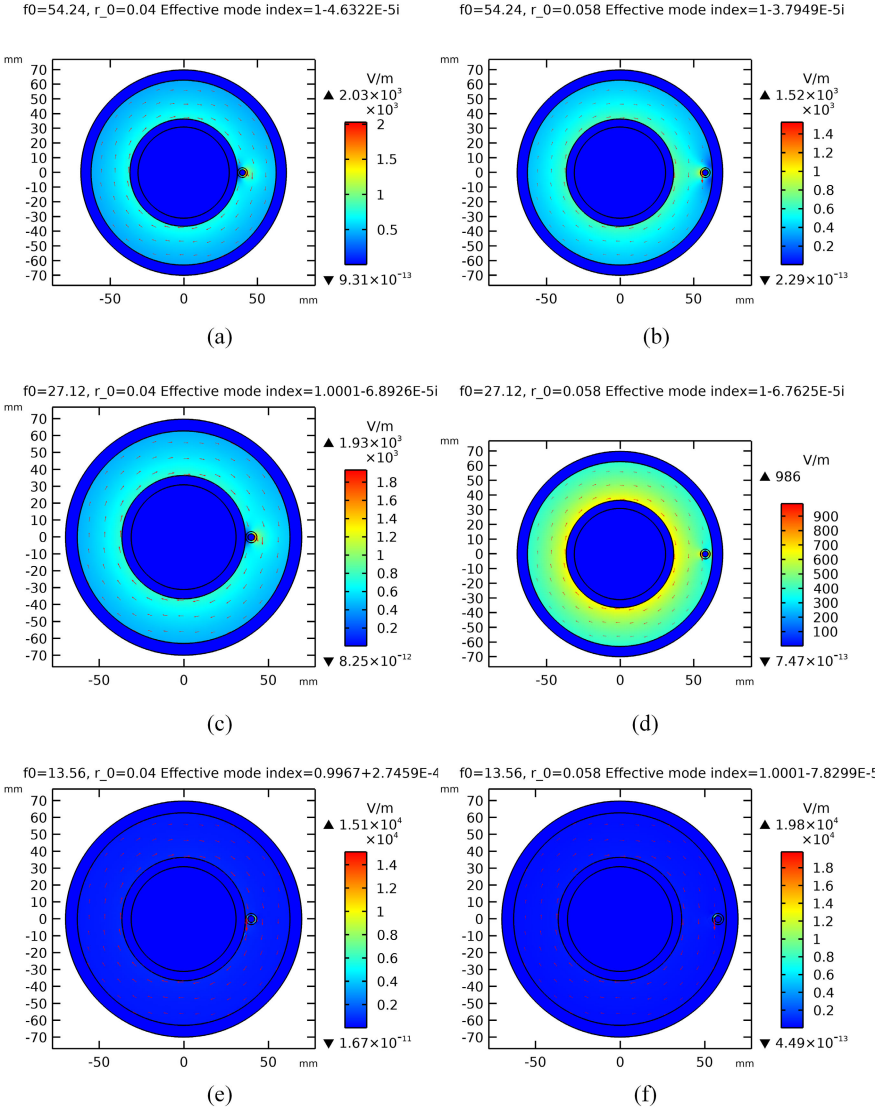

FIGURE 13. EM field distribution with tubing and casing bias corresponding to $r_0 = 0.04$ and $r_0 = 0.058$ respectively (a) $f_0 = 54.24$ MHz with EMI $= 1 - 4.6322e - 5i$ (b) $f_0 = 54.24$ MHz with EMI $= 1 - 3.794e - 5i$ (c) $f_0 = 27.12$ MHz with EMI $= 1 - 6.8926e - 5i$ (d) $f_0 = 27.12$ MHz with EMI $= 1 - 6.7625e - 5i$ (e) $f_0 = 13.56$ MHz with EMI $= 0.9967 + 2.7459e - 4i$ (f) $f_0 = 13.56$ MHz with EMI $= 1 - 7.8299e - 5i$.

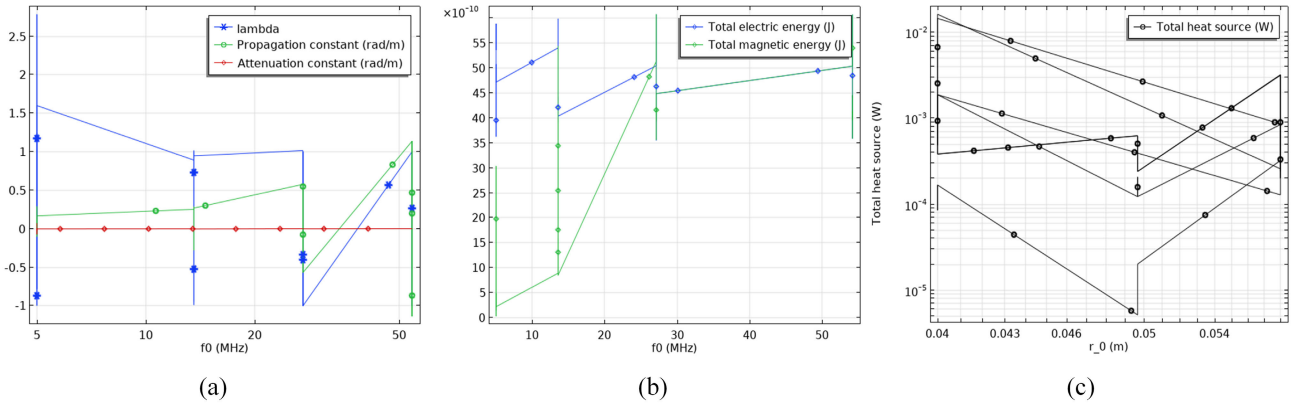

FIGURE 14. Wave propagation characteristics at eigenfrequency (a) Wavelength, propagation and attenuation plots over IHRFB (b) Total electric and magnetic energy profile (c) Total heat source vs r_0 position.

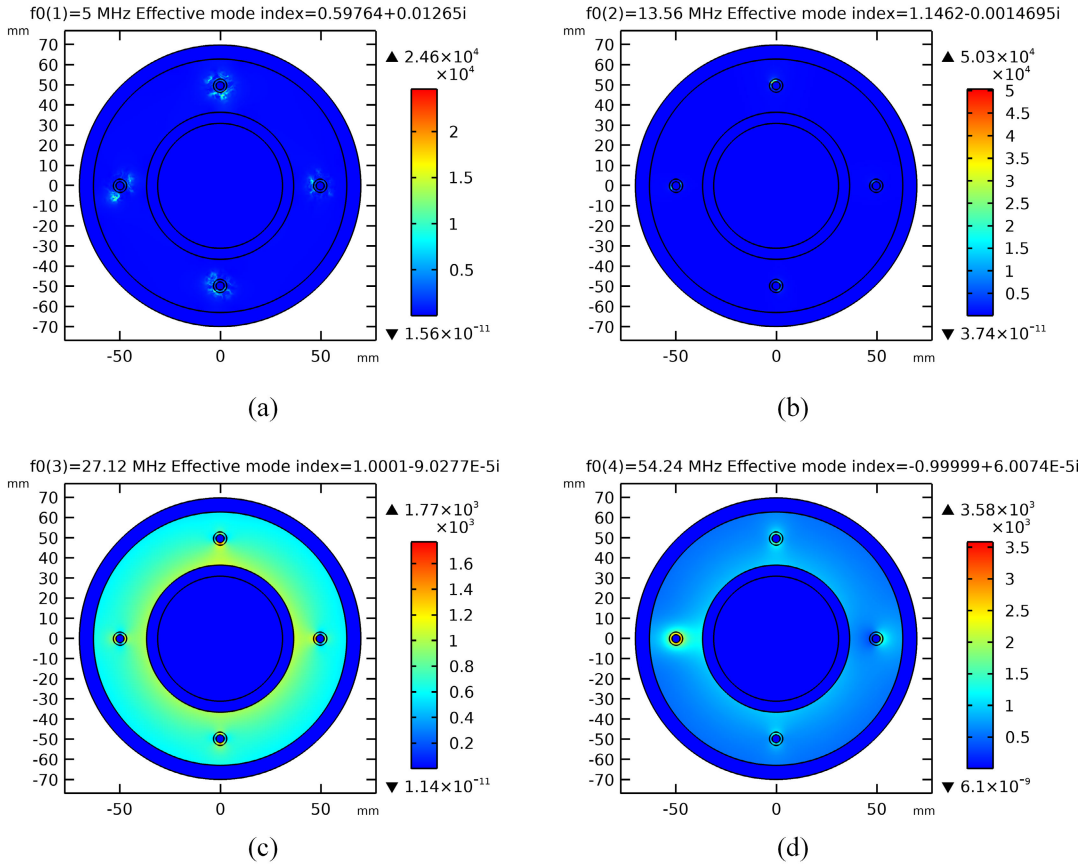

FIGURE 15. EM field distribution in 4−element TL tubular at effective modes near 1(a) $f_0 = 5$ MHz with EMI= $0.59764 + 0.01265i$ (b) $f_0 = 13.56$ MHz with EMI= $1.1462 - 0.0014695i$ (c) full resonant mode obtained at $f_0 = 27.12$ MHz with EMI= $1 - 9.0277e - 5i$ (d) partial resonance obtained at $f_0 = 54.24$ MHz and EMI= $-0.999 + 6.007e - 5i$.

cylindrical waveguide obtained by inserting the coaxial RH-TL, the electric field distribution is represented by the blue region while the red arrows present the magnetic field distribution and polarization. The size of the arrow suggests the magnitude of the tangential magnetic field vector whereas the direction correlates with the polarization. Figure 12 and Figure 13 present the EM field distribution for a single coaxial RH-TL in the well tubular waveguide at modes near vacuum refractive index for neutral case $R_w = r_0 = 0.049685$ m and bias case $R_w \neq r_0$ respectively. For the neutral case where the TL is positioned at the midpoint between inner casing and outer tubing surfaces, with a slight change in the imaginary part of the EMI, a resonance mode is triggered. While in resonance, the electric field intensity decreases significantly from $5.75e3$ to $1.05e3$ V/m as presented in Figure 12(e) and (f) for 27.12 MHz and from $5.52e3$ to $1.82e3$ V/m as shown in Figure 12(g) and (h) for the 54.24 MHz resonance frequency. For the bias cased presented in Figure 13(a) to (f), resonant modes were found at 27.12 MHz and 54.24 MHz for both tubing bias $r_0 = 0.04$ m and casing bias $r_0 = 0.058$ m. At $r_0 = 0.04$ m, partial resonance is observed with the electric field intensity highest around the TL with values of $2.03e3$ V/m at 54.24 MHz and $1.93e3$ V/m at 27.12 MHz. Whereas, at $r_0 = 0.058$ m, full resonance was observed at 27.12 MHz and partial resonance at 54.24 MHz with high intensity of 986 V/m and $1.52e3$ V/m respectively along the tubing surfaces as seen in Figure 13(b) and (d). This condition is suitable for intentional heating of tubing to mitigate the glass transition phase of flowing fluid in the tubing. Figure 14 presents the wave propagation and attenuation profiles for the well tubular waveguide. It is observed that at resonant modes over the IHRFB, the wavelengths and propagation constants are identical as seen in Figure 14(a). The resulting total wave energy is presented in Figure 14(b). The correlation between the r_0 and the total heat dissipation is established with higher values along the biased positions at $r_0 = 0.04$ m and $r_0 = 0.058$ m. The highest values of the heat source along the tubing due to coupling in resonant modes are consistent. In the 4-element array scenario presented in Figure 15(a) to (d), the resonant modes are consistent with 27.12 MHz presenting full resonance while partial resonance from one array element was found at 54.24 MHz. The maximum intensity values are $1.77e3$ V/m and $3.58e3$ V/m respectively.

C. EFFECT OF IDEAL REACTANCES ON LEFT-HANDED TRANSMISSION FREQUENCY

To obtain the left-handedness of the coaxial RH-TL over the IHRFB, the lumped element values were computed for the

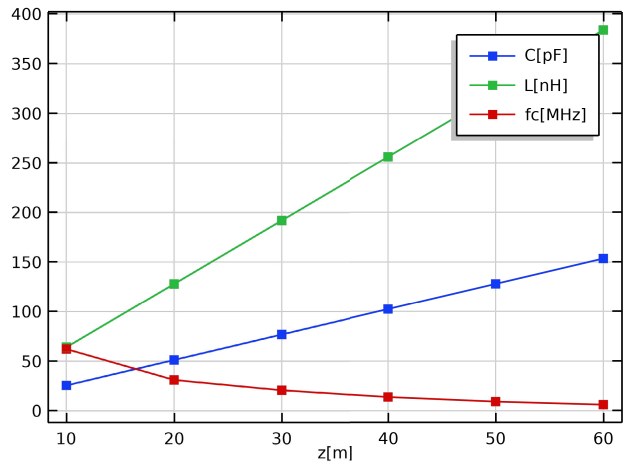

FIGURE 16. Left-handed transmission line parameters.

cut-off frequencies. A linear proportionality is established between both per unit inductances and capacitances with the depth of the line. For IHRFB, the per unit length values of 2.56 pF/m and 6.4 nH/m was obtained with the cuf-off frequency range of 62.17 MHz to 6.13 MHz both within the IHRFB. Although the evaluated lumped element capacitances and inductances presented in Figure 16 are valid with f_c within the IHRFB for depths up to 60 m, further evaluation of line parameters will yield more precise frequency values where non-resonant modes are required for coupling to an antenna array. For depths beyond 60 m, range extension within the IHRFB is achievable with implementation of the LH-TL circuit and components [52], [53]. The approach developed in this study considered the well tubular structure as a waveguide consisting of concentric cylindrical tubing and casing with the transmission line as a wave excitation source in the middle of the air-filled dielectric medium. By evaluating the EM fields within the annular space, reactive coupling was identified and mitigated. Since the application domain for RF-EM heating is primarily reservoirs with thin pay-zones where conventional EOR methods are less desirable, this approach becomes considerable. By considering that the pay-zone is a porous dielectric medium bounded at the top and bottom by the overburden and underburden respectively, the waveguide approach of wave propagation analysis will be valid by assuming that the layers have homogeneous permeability and permittivity. This by analogy, creates a waveguide of a heavy oil porous media and conducting surfaces made of solid rock. Effectively, the resonance modes for antenna wave propagation can be identified using resonance analysis. In contrast to the wave transmission scenario, identifying the resonance modes in antenna propagation will optimize the heating regime. To minimize losses due to dispersion, metamaterial RF antenna with effective matching to the LH-TL will be required to propagate EM waves over large radial distances on the reservoir pay-zone. The need for dynamic variation of the propagation frequency has been associated with the response of the porous medium to the EM fields. At lower frequencies, the frequency of dielectric polarization is greatly influenced by the viscosity of the medium. Meanwhile at higher frequencies, the attenuation of the waves become higher and the penetration is compromised. This necessitates a trade-off between the depth of effective penetration and the rate of energy exchange. The solution of which is in the dynamic regulation of propagation frequency in line with the absorption frequency of the porous medium especially within the identified industrial heating frequency band.

D. RESONANCE HEATING IN POROUS MEDIUM

In particular, scenarios where reservoir conductivity and permittivity are modified by the injection of nanoparticles, resonance heating will enhance the attainment of high volumetric temperatures due to the frequency-dependent complex permeability and permittivity of the conductive molecules within the EM fields. In line with the results obtained for the resonance modes of the RH-TL, the variation of frequencies from 13.56 MHz for increased propagation can be varied to 54.24 MHz to stimulate potential resonance modes. The prevalence of resonance modes at 54.24 MHz is consistent with the frequency utilized in the Ion Cyclotron Resonance Heating (ICRH). In terms of the effect of enhanced RF power transmission on the enhancement of oil recovery, efficiency values of less than 50 % have contributed to poor adoption of the technique. To measure the effect of increased efficiency [54], [55], the form factor K_{em} is a major parameter [45]. Defined as the ratio of the energy contained in produced heavy oil to the energy consumed by the antenna, the form factor provides a time dependent evaluation of the contributions of power transmission losses to the recovery of heavy oil by electromagnetic heating.

VI. CONCLUSION

The enhancement of RF power transmission was investigated in this study by considering an extrinsic well tubular waveguide and a left-handed transmission line approach. In the waveguide approach, the excitation source, (RH-TL) placed in the wellbore at various $r-axis$ positions was analysed. The frequency modal analysis was conducted on the well tubular structure to determine the resonant frequencies leading to coupling of EM fields over the IHRFB for an effective mode index close to 1 (near refractive index of a vacuum). A two level mesh refinement study presented insignificant changes in the electromagnetic coupling. However, it provided increased precision in the complex EMI values. The characteristic impedance of the coaxial RH-TL was evaluated and the relationship between frequency and impedance was established. In the concentric cylindrical well tubular waveguide, it was observed that resonant modes were absent at lower transmission frequencies below 13.56 MHz. However, at 27.12 MHz, full resonance mode was identified. Partial resonance was observed at 54.24 MHz. This will enable the mitigation of coupling during power transmission. By using ideal elements capacitances and inductances, the permeability and permittivity of the RH-TL was modified to achieve

left-handedness; thereby, achieving an artificial power line over the IHRFB. Consequently, RF power transmission over large depths of a reservoir can be achieved using artificial power lines and selecting a suitable mode of EM wave propagation.

A. RECOMMENDATIONS FOR FUTURE WORK

This work presents an eigenfrequency resonance study of a 2-dimensional model of a vertical well tubular structure excited by a coaxial transmission line at pre-production stage. Further study is required to determine the response of the tubulars when heavy oil is produced through the tubing at varying levels of excitation. A 3D simulation of the power transmission will enhance the understanding of the power losses incurred. Subsequently, a field test is recommended to test the implementation of artificial power lines for enhanced efficiency of downhole RF power transmission.

VII. ABBREVIATIONS AND ACRONYMS

ARPACK	Arnoldi Package
APL	Artificial Power Line
BE	Boundary Elements
DE	Domain Elements
DoF	Degrees of Freedom
EEOR	Electrothermal enhanced oil recovery
EM	Electromagnetic
EMH	Electromagnetic Heating
EMI	Effective mode index
EOR	Enhanced Oil Recovery
ICRH	Ion Cyclotron Resonance Heating
IHRFB	Industrial Heating Radiofrequency Band
LH	Left-handed
LH-TL	Left-handed transmission line
NoE	Number of Elements
OOIP	Original Oil in Place
OCS	Optimal Casing Size
OTS	Optimal Tubing Size
RES	Renewable Energy Sources
RF	Radiofrequency
RFG	Radiofrequency Generator
RH	Right-handed
RH-TL	Right-handed transmission line
SWR	Standing Wave Ratio
TE	Transverse Electric
TEM	Transverse Electric and Magnetic
TL	Transmission Line
TM	Transverse Magnetic

APPENDIX A

Partially reflected and absorbed power occurs due to mismatch in purely resistive or for complex loads. For passive loads ($Z_L = R + j\chi$, with $R > 0$) the modulus of the reflection coefficient is $|\rho_L| \leq 1$. This is expected since the reflected power, given by:

$$P^- = \frac{I\left|V_o^+\right|^2}{2\,Z_o}\,|\rho_L|^2 \tag{A.38}$$

cannot be higher than the incident power for passive loads. The reflection coefficient, known as return loss, is typically expressed in dB and given by:

$$RL = -20log\,|\rho_L| \tag{A.39}$$

For infinitely long TLs or those terminated with a matched load, constant amplitude travelling waves are present in the line. However, if a reflected wave is generated in the load plane, a standing wave is generated in the line, where the amplitude is modulated by the modulus of the reflection coefficient. Then the voltage in the line becomes:

$$V\,(z) = V_o^+\left[e^{-j\beta z} + \rho_L e^{j\beta z}\right] \tag{A.40}$$

with the reflection coefficient expressed in polar form $\left(\rho_L = |\rho_L|\,e^{j\theta}\right)$, the voltage in the line can be written as:

$$V\,(z) = V_o^+ e^{-j\beta z}\left[1 + |\rho_L|\,e^{2j\beta z + j\theta}\right] \tag{A.41}$$

from which it follows that:

$$|V\,(z)|^2 = \left|V_o^+\right|^2\left[1 + |\rho_L|^2\,2\,|\rho_L|\,cos\,(2\beta z + \theta)\right] \tag{A.42}$$

Equation A.42 indicates that the amplitude is a maximum $\left(V_{max} = \left|V_o^+\right|[1 + |\rho_L|]\right)$ and a minimum $\left(V_{min} = \left|V_o^+\right|[1 - |\rho_L|]\right)$ at planes separated by $\lambda/4$, and the ratio between the maximum and minimum voltage in the line, known as voltage standing wave ratio, is given by:

$$SWR = \frac{1 + |\rho_L|}{1 - |\rho_L|} \tag{A.43}$$

As anticipated, the SWR is determined by the reflection coefficient. However, it only depends on the modulus of the reflection coefficient, not on its phase, θ. This means that from the information of the SWR, it is not possible to completely characterize the load. For instance, it is not possible

TABLE 8. Typical Values of Heat losses from bare metal pipe insulation.

Surface Area heat loss at				Units
Conditions	93°C	204°C	316°C	J/m^2s
still air, 0°F	1620	4680	9360	
still air, 100°F	630	2970	6750	
10-mph wind, 0°F	3030	7620	14040	
10-mph wind, 100°F	1320	5130	10500	
40-mph wind, 0°F	4860	12360	22320	
40-mph wind, 100°F	2100	8280	16950	

TABLE 9. Typical Values of heat losses from Magnesia pipe insulation, air temperature 27°C.

Surface Area heat loss at					Units
Dimensions	93°C	204°C	316°C	427°C	J/m-s
Standard on 3-in pipe	45.5	136.5	245.7	400.4	
Standard on 6-in pipe	70.07	211.12	379.47	564.2	
1.5-in. on 3-in pipe	36.4	104.65	188.37	300.3	
1.5-in. on 6-in pipe	58.24	169.26	304.85	452.27	
3 in on 3-in pipe	21.84	68.25	122.85	182	

to distinguish between a short circuit, an open circuit, or a reactive load, since the reflection coefficient of these loads has the same modulus ($|\rho_L| = 1$).

APPENDIX B

See Tables 8 and 9.

TABLE 10. Common Production Casing Diameters.

Nominal (in.)	Outer (mm)	Thickness (mm)
$4\frac{1}{2}$	114.3	5.21, 6.35, 7.37, 8.56
5	127	5.59, 6.43, 7.52, 9.20
$5\frac{1}{2}$	139.7	6.20, 6.98, 7.72, 9.17, 10.54
$6\frac{5}{8}$	168.3	7.32, 8.94, 10.59, 12.07
7	177.8	5.87, 6.91, 8.05, 9.20, 10.36, 11.51, 12.65
$7\frac{5}{8}$	193.7	7.62, 8.33, 9.93, 10.92, 12.70

TABLE 11. Nominal Tubing Diameters.

Nominal [mm (in.)]	Inside (mm)	Outside (mm)	Thickness (mm)
33.4 (1.315)	26.4	33.4	7
42.2 (1.660)	35.2	42.2	7
48.3 (1.900)	40.3	48.3	8
60.3 ($2\frac{3}{8}$)	50.7	60.3	9.6
73.0 ($2\frac{7}{8}$)	62	73	11
88.9 ($3\frac{1}{2}$)	75.9	88.9	13
101.6 (4)	90.1	101.6	11.5

REFERENCES

[1] A. Philip, F. Freeman R. Meyer, and D. Attanasi, "Natural bitumen resources in geological basins of the world," *U. S. Geolog. Surv.*, vol. 1084, pp. 1–36, 2007.
[2] B. Y. Jamaloei, "Electromagnetic heating for heavy-oil and bitumen recovery: Experimental, numerical, and pilot studies," *SPE Reservoir Eval. Eng.*, vol. 25, pp. 433–454, Mar. 2022.
[3] Q. Zhang, W. Liu, and A. D. Taleghani, "Numerical study on non-newtonian Bingham fluid flow in development of heavy oil reservoirs using radiofrequency heating method," *Energy*, vol. 239, Jan. 2022, Art. no. 122385.
[4] M. Ismail, G. Gao, I. Sajid, and Y. Wang, "A review of techniques for enhancing oil recovery by EM and US wave," in *Proc. Int. Field Explor. Develop. Conf.* Cham, Switzerland: Springer, 2018, pp. 1604–1615.
[5] A. Bera and T. Babadagli, "Effect of native and injected nano-particles on the efficiency of heavy oil recovery by radio frequency electromagnetic heating," *J. Petroleum Sci. Eng.*, vol. 153, pp. 244–256, May 2017.
[6] U. Abdulkadir, J. Hashim, M. Alkali, and A. Kumar, "Application of thermal methods for heavy oil recovery: Phase one," *Int. J. Advance Res. Develop.*, vol. 2, no. 5, pp. 102–120, 2017.
[7] H. Ritchey, "Radiation heating," U.S. Patent 2 757 738, Aug. 7, 1956.
[8] I. Bogdanov, S. Cambon, and C. Prinet, "Analysis of heavy oil production by radio-frequency heating," in *Proc. SPE Int. Heavy Oil Conf. Exhib.*, 2014, doi: 10.2118/172862-MS.
[9] G. M. Wallace, "Heating and current drive actuators study for FNSF in the ion cyclotron and lower hybrid range of frequency," *Fusion Eng. Des.*, vol. 135, pp. 370–379, Oct. 2018.
[10] A. Borthwick, G. Agarici, A. Davis, P. Dumortier, F. Durodie, J. Fanthome, C. Hamlyn-Harris, A. D. Hancock, D. Lockley, R. Mitteau, M. Nightingale, R. Sartori, and K. Vulliez, "Mechanical design features and challenges for the ITER ICRH antenna," *Fusion Eng. Des.*, vol. 84, nos. 2–6, pp. 493–496, Jun. 2009.
[11] F. Braun, "Stability problems of high power ion cyclotron resonance heating systems," *Fusion Eng. Des.*, vol. 30, no. 3, pp. 233–244, Jul. 1995.
[12] S. R. Shewale, D. Rajoriya, M. L. Bhavya, and H. U. Hebbar, "Application of radiofrequency heating and low humidity air for sequential drying of apple slices: Process intensification and quality improvement," *LWT*, vol. 135, Jan. 2021, Art. no. 109904.
[13] A. Altemimi, S. N. Aziz, A. R. S. Al-HiIphy, N. Lakhssassi, D. G. Watson, and S. A. Ibrahim, "Critical review of radio-frequency (RF) heating applications in food processing," *Food Quality Saf.*, vol. 3, no. 2, pp. 81–91, Jun. 2019.
[14] Z. Huang, F. Marra, and S. Wang, "A novel strategy for improving radio frequency heating uniformity of dry food products using computational modeling," *Innov. Food Sci. Emerg. Technol.*, vol. 34, pp. 100–111, Apr. 2016.
[15] M. Hiraoka, M. Mitsumori, N. Hiroi, S. Ohno, Y. Tanaka, Y. Kotsuka, and K. Sugimachi, "Development of RF and microwave heating equipment and clinical applications to cancer treatment in Japan," *IEEE Trans. Microw. Theory Techn.*, vol. 48, no. 11, pp. 1789–1799, Nov. 2000.
[16] Y. Xu, M. Mahmood, Z. Li, E. Dervishi, S. Trigwell, V. P. Zharov, N. Ali, V. Saini, A. R. Biris, D. Lupu, D. Boldor, and A. S. Biris, "Cobalt nanoparticles coated with graphitic shells as localized radio frequency absorbers for cancer therapy," *Nanotechnology*, vol. 19, no. 43, Oct. 2008, Art. no. 435102.
[17] J. Sun, A. Zhang, and L. X. Xu, "Evaluation of alternate cooling and heating for tumor treatment," *Int. J. Heat Mass Transf.*, vol. 51, nos. 23–24, pp. 5478–5485, Nov. 2008.
[18] Z. Wang and D. Gao, "A simulation study on the high-frequency electromagnetic heating heavy oil reservoir and analysis of influencing factors," *Arabian J. Sci. Eng.*, vol. 44, no. 12, pp. 10547–10559, Dec. 2019.
[19] A. Davletbaev, L. Kovaleva, and T. Babadagli, "Combining solvent injection, electromagnetic heating, and hydraulic fracturing for multi-stage heavy oil recovery," *J. Electromagn. Waves Appl.*, vol. 30, no. 2, pp. 207–224, Jan. 2016.
[20] A. Bera and T. Babadagli, "Status of electromagnetic heating for enhanced heavy oil/bitumen recovery and future prospects: A review," *Appl. Energy*, vol. 151, pp. 206–226, Aug. 2015.
[21] M. M. Rehman and M. Meribout, "Conventional versus electrical enhanced oil recovery: A review," *J. Petroleum Explor. Prod. Technol.*, vol. 2, no. 4, pp. 157–167, Dec. 2012.
[22] A. Mukhametshina and E. Martynova, "Electromagnetic heating of heavy oil and bitumen: A review of experimental studies and field applications," *J. Petroleum Eng.*, vol. 2013, pp. 1–7, Apr. 2013.
[23] M. Kashif, N. Nasir, M. N. Akhtar, and N. Yahya, "Experimental study of electromagnetic waves affects on enhanced oil recovery," in *Proc. Nat. Postgraduate Conf.*, Sep. 2011, pp. 1–4.
[24] L. Kovaleva, A. Davletbaev, T. Babadagli, and Z. Stepanova, "Effects of electrical and radio-frequency electromagnetic heating on the mass-transfer process during miscible injection for heavy-oil recovery," *Energy Fuels*, vol. 25, no. 2, pp. 482–486, Feb. 2011.
[25] M. Bientinesi, L. Petarca, A. Cerutti, M. Bandinelli, M. D. Simoni, M. Manotti, and G. Maddinelli, "A new technique for heavy oil recovery based on electromagnetic heating: Pilot scale experimental validation," *Chem. Eng. Trans.*, vol. 32, 2013.
[26] R. S. Kasevich, S. L. Price, D. L. Faust, and M. F. Fontaine, "Pilot testing of a radio frequency heating system for enhanced oil recovery from diatomaceous earth," in *Proc. SPE Annu. Tech. Conf. Exhib.*, Sep. 1994, pp. 105–119.
[27] Z. Wang, D. Gao, K. Liu, T. Tan, Z. Wang, and W. Li, "Study on radio frequency heating pattern of heavy oil reservoir based on multi-antenna configuration," in *Proc. SPE Int. Heavy Oil Conf. Exhib.*, 2018, doi: 10.2118/193774-MS.
[28] G. Li, X. Guan, H. Wang, S. Du, D. Wu, and J. Chen, "Simulation of radio frequency heating of heavy oil reservoir using multi-physics coupling of reservoir simulation with electromagnetic solver," in *Proc. SPE Reservoir Simul. Conf.*, 2019, doi: 10.2118/193836-MS.
[29] Z. Wang, D. Gao, and J. Fang, "Numerical simulation of RF heating heavy oil reservoir based on the coupling between electromagnetic and temperature field," *Fuel*, vol. 220, pp. 14–24, May 2018.
[30] A. Saeedfar, D. Lawton, and K. Osadetz, "Directional RF heating for heavy oil recovery using antenna array beam-forming," in *Proc. SPE Canada Heavy Oil Tech. Conf.*, 2016, doi: 10.2118/180695-MS.
[31] M. Hosseinpour, M. Soltani, and J. Nathwani, "Renewable energy integration with hot compressed water in heavy oil upgrading: A practice toward sustainability," *J. Cleaner Prod.*, vol. 334, Feb. 2022, Art. no. 130268.
[32] Y. Choi, C. Lee, and J. Song, "Review of renewable energy technologies utilized in the oil and gas industry," *Int. J. Renew. Energy Res.*, vol. 7, no. 2, pp. 592–598, 2017.
[33] T. Batal, R. Ragona, J. Hillairet, C. Yu, J.-M. Bernard, P. Mollard, F. Farina, M. Firdaouss, and Q. Yang, "Design and thermal-structural analysis of a high power ICRH travelling wave array antennas," *Fusion Eng. Des.*, vol. 166, May 2021, Art. no. 112325.
[34] K. Saito, S. J. Wang, H. H. Wi, H. J. Kim, S. Kamio, G. Nomura, R. Seki, T. Seki, H. Kasahara, and T. Mutoh, "Development of power combination system for high-power and long-pulse ICRF heating in LHD," *Fusion Eng. Des.*, vol. 146, pp. 256–260, Sep. 2019.

[35] V. I. Malarev, A. V. Kopteva, and V. Y. Koptev, "Electric power supply system development for down-hole electric steam generators to produce high-viscosity oil," in *Proc. Int. Multi-Conf. Ind. Eng. Modern Technol. (FarEastCon)*, Oct. 2018, pp. 1–4.
[36] A. A. Belsky and V. S. Dobush, "Oil well electrical heating facility utilizing heating cable powered by autonomous wind-driven power unit," in *Proc. Dyn. Syst., Mech. Mach. (Dynamics)*, Nov. 2016, pp. 1–4.
[37] M. M. Medizade and Z. Wiltshire, "Further investigation of downhole heating by an electric cable," in *Proc. SPE Western Regional Meeting*, Apr. 2019, Art. no. D041S014R002.
[38] C. Caloz and T. Itoh, "Transmission line approach of left-handed (LH) materials and microstrip implementation of an artificial LH transmission line," *IEEE Trans. Antennas Propag.*, vol. 52, no. 5, pp. 1159–1166, May 2004.
[39] A. F. Abdelaziz, T. M. Abuelfadl, and O. L. Elsayed, "Realization of composite right/left-handed transmission line using coupled lines," *Electr. Eng.*, vol. 92, pp. 299–315, Jan. 2009.
[40] R. Yusupov, E. Meretskaya, A. Cheremisin, and D. Eskin, "Modeling steam flow in an injection tubing and analysis of flow regimes for high pressure-high temperature initial parameters," *Chem. Eng. Process.-Process Intensification*, vol. 158, Dec. 2020, Art. no. 108168.
[41] C. C. Nwanwe, U. I. Duru, O. I. Nwanwe, A. O. Chikwe, K. T. Ojiabo, and C. T. Umeojiakor, "Optimum tubing size prediction model for vertical multiphase flow during flow production period of oil wells," *J. Petroleum Explor. Prod. Technol.*, vol. 10, no. 7, pp. 2989–3005, Oct. 2020.
[42] W. Rempu, "Selection and determination of tubing and production casing sizes," in *Advanced Well Completion Engineering*. Gulf Professional Publishing, 2011, pp. 117–170.
[43] W. Renpu, "Well completion mode selection," in *Advanced Well Completion Engineering*. Gulf Professional Publishing, 2011, pp. 75–116.
[44] F. Yeh and C. Shimabukuro, *The Essence of Dielectric Waveguides*. Springer, 2008.
[45] A. Davletbaev, L. Kovaleva, and T. Babadagli, "Mathematical modeling and field application of heavy oil recovery by radio-frequency electromagnetic stimulation," *J. Petroleum Sci. Eng.*, vol. 78, nos. 3–4, pp. 646–653, Sep. 2011.
[46] L. A. Strelets and S. O. Ilyin, "Effect of enhanced oil recovery on the composition and rheological properties of heavy crude oil," *J. Petroleum Sci. Eng.*, vol. 203, Aug. 2021, Art. no. 108641.
[47] F. Martín, "Fundamentals of planar transmission lines," *Artificial Transmission Lines for RF and Microwave Applications*. 2015, pp. 1–46.
[48] M. Notomi, "Theory of light propagation in strongly modulated photonic crystals: Refractionlike behavior in the vicinity of the photonic band gap," *Phys. Rev. B, Condens. Matter*, vol. 62, no. 16, pp. 10696–10705, Oct. 2000.
[49] I. Llamas-Garro, M. J. Lancaster, and P. S. Hall, "Air-filled square coaxial transmission line and its use in microwave filters," *IEE Proc.-Microw., Antennas Propag.*, vol. 152, no. 3, pp. 155–159, Jun. 2005.
[50] F. Sepaintner, A. Scharl, J. Jakob, F. Keck, K. Kunze, F. X. Rohrl, W. Bogner, and S. Zorn, "Cost-effective implementation of air-filled waveguides on printed circuit boards," in *Proc. IEEE 29th Conf. Electr. Perform. Electron. Packag. Syst. (EPEPS)*, Oct. 2020, pp. 2020–2022.
[51] X. Cheng, T. Xie, Y. Yao, Y. Yang, T. Zhang, J. Yu, and X. Chen, "Contactless air-filled mode selective transmission line," *IEEE Microw. Wireless Compon. Lett.*, vol. 32, no. 11, pp. 1291–1294, Nov. 2022.
[52] A. Cherepanov, A. Dobrikov, and A. Zagorodny, "Dynamic range extension method for microwave power meters," in *Proc. ITM Web Conferences*, vol. 30, 2019, p. 11004.
[53] M. Zafar, S. Ekpo, J. George, P. Sheedy, M. Uko, and A. Gibson, "Hybrid power divider and combiner for passive RFID tag wireless energy harvesting," *IEEE Access*, vol. 10, pp. 502–515, 2022.
[54] X. Liang, J. Stevens, and D. Kelly, "Subsea cable applications in offshore oilfield facilities," in *Proc. Soc. Petroleum Eng.-SPE Offshore Eur. Conf. Exhib.*, 2013, pp. 156–167.
[55] C. K. Chung, D. Cox, L. Dalrymple, B. Yingst, and J. Russell, "Latest development and project utilization of heater cable in ESP production system," in *Proc. SPE Prod. Oper. Symp.*, Mar. 2011, pp. 433–449.

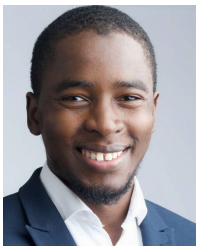

ADAMU A. ADAMU (Student Member, IEEE) received the B.Sc. degree in electrical engineering and the M.Sc. degree in environmental engineering from the Warsaw University of Technology, Poland, in 2012 and 2014, respectively. He is currently pursuing the Ph.D. degree in engineering with the University of Aberdeen, U.K. His research interest includes the improvement of radio-frequency electromagnetic heating for enhanced recovery of heavy oil.

PRASHANT S. JADHAWAR received the B.Eng. and M.Eng. degrees in petroleum engineering from the University of Pune, India, in 1996 and 2000, respectively, the M.Phil. degree in petroleum engineering from Heriot-Watt University, in 2005, and the Ph.D. degree in petroleum engineering from the University of Adelaide, in 2010, with specialization in CO2-assisted gravity drainage EOR process: reservoir simulation and scaled model studies. He has more than 18 years work experience of teaching (14 years) plus oil and gas industry (four years) in U.K., Germany, Australia, and India, with expertise in enhanced oil and gas recovery, CO2 sequestration combined with EOR/EGR, reservoir modeling and simulation, and reservoir fluid characterization/PVT phase behavior and flow assurance (hydrate, wax, and asphaltenes). Prior to the University of Aberdeen, he had been a Senior Reservoir Engineer Research and Development (EOR) at Wintershall Holding GmBH, Germany. He has published around 20 technical papers and written several technical reports. Over the years, he taught numerous courses, including reservoir engineering, reservoir simulation, PE reservoir fluid properties/thermodynamics, enhanced oil recovery (EOR), and surface production systems. He is also a member of SPE and IET and an Associate Member of the *Journal of the Energy Institute*. He is also an Editorial Board Member of *Nature* (Springer) and a reviewer for numerous journals.

SUMEET S. APHALE (Senior Member, IEEE) received the B.Eng., M.S., and Ph.D. degrees in electrical engineering with a focus on Robotics and Control, in 1999, 2003, and 2005, respectively. He is currently a Reader at the School of Engineering, University of Aberdeen, U.K., where he is also the Director of the Artificial Intelligence, Robotics and Mechatronic Systems Group (ARMS). He has published over 100 peer-reviewed journals and conference papers reporting novel results in mechatronics, robotics, and control engineering. His research interests include control engineering, mechatronic systems, and robotics where he focuses on devising accurate system models and simple but well-performing control schemes that deliver vibration suppression/isolation, accurate positioning, and robustness to parameter uncertainty. He is an Associate Editor of IEEE Control Systems Letters and *Frontiers in Mechanical Engineering—Mechatronics*; along with several other editorial and technical committee appointments.